DINAME 2017 - Proceedings of the XVII International Symposium on Dynamic Problems of Mechanics
A. T. Fleury, D. A. Rade, P. R. G. Kurka (Editors), ABCM, São Sebastião, SP, Brazil, March 5-10, 2017

Numerical and Experimental Analysis of a Parallel 2 DOF Manipulator

William Schroeder Cardozo[1], **Hans Ingo Weber**[1]

[1] PUC-Rio R. Marquês de São Vicente, 225, RJ - Brasil, billi83@globo.com, hans@puc-rio.br

Abstract: A parallel two degrees of freedom manipulator designed for a variable orientation of a body in space is analyzed. The manipulator consists of one universal joint with one axis fixed to the base and the other axis fixed to a moving platform. A similar device is used in spacecrafts to orient the rocket nozzle. In this work, two parallel linear hydraulic actuators move the platform. A novel proportional digital hydraulic valve is used to control the actuators. Each fork of the universal joint has an angular position sensor mounted to measure the relative motion of the cross. An inertial measurement unit (IMU) is fixed to the moving platform. Load cells and pressure transducers are mounted on the actuators to measure force and chambers pressure. Numerical simulations are presented using a desired trajectory as input for a proportional controller (P-controller). An experimental apparatus is used to validate the numerical results.

Keywords: Kinematics, Electrohydraulic Servosystem, Servoactuator, Universal Joint, IMU

INTRODUCTION

A platform is designed with two linear hydraulic actuators mounted around a universal joint, thus forming a parallel manipulator with two degrees of freedom (2dof). Fig. 1 shows the concept of this device with a load over the moving platform. The hydraulic actuators are connected to the base through smaller universal joints and to the moving platform through ball joints.

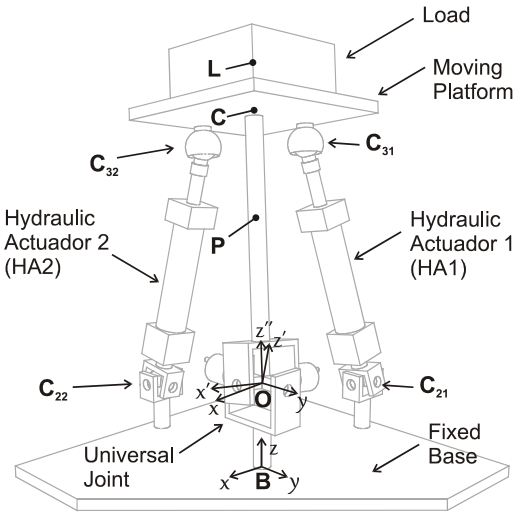

Figure 1 – Kinematic scheme.

The thrust vector control (TVC) scheme is similar to this platform and orients the rocket nozzle in spacecraft. The (TVC) produces torque around the center of mass of the spacecraft in order to steer and keep it on the desired flight path (Wekerle, et al., 2016). Unlike constant velocity joints, like Rzeppa or Thomson coupling, the universal joint generates angular acceleration at the output axis in relation to the input axis (Watson, et al., 2013). The consequence of this acceleration is analyzed in this work. For simpler kinematics analysis, the actuators are equal and its mounting points are symmetric (Taghirad, 2013). Hydraulic actuators are chosen due to their high power to weight ratio, good controllability and self lubrication property.

Wekerle, et al. (2015), presents the requirements of an actuation system for TVC systems and presents in (2016) a 2-dof mockup of a rocket motor nozzle with two electrohydraulic actuators. The actuators performances are identified in a mass-spring test bench.

Ghosh et al. (2015) developed a 2-dof parallel hydraulic actuated system for a heave and pitch motion simulator. Two low-cost commercial solenoid proportional valves control the hydraulic actuators. These kind of valves have a

dead-band and non-linear behavior. Ghosh et al. have tried different types of controllers, and the self-tuning fuzzy proportional–integral–derivative (PID) with bias control showed the best performance. The PID controller had the worst response.

In this work, a novel proportional digital hydraulic valve (PDHV) controls the oil flow in the hydraulic actuators chambers. The proposed PDHV has much lower price and less contamination sensitivity, when compared with a commercial sliding spool servovalve. However, the PDHV is low-bandwidth modulating. Numerical and experimental trials validate the proposed system.

The test bench has an angular position sensor on each fork of the universal joint to measure the relative motion of the cross. An inertial measurement unit (IMU) measures the embarked angular velocity of the moving platform and the linear acceleration of a point. Moreover, load cells and pressure transducers mounted on the actuators measure the force and the chambers pressure.

Hydraulic Control System

Each platform actuator is controlled by one PDHV, as shown in Fig. 2. Changing the valve rotor angle θ_V the pressure drop and flow rate trough the valve changes. It changes the pressure in the pipeline and in the actuator chambers, which generate a force that moves the piston.

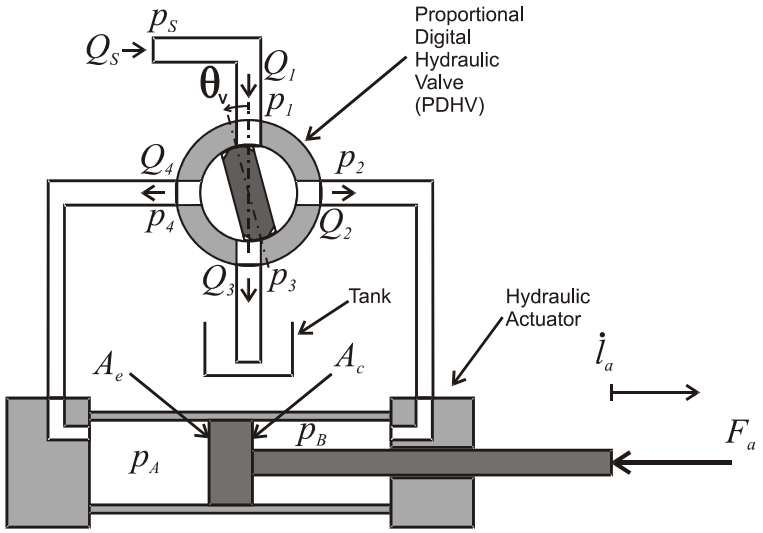

Figure 2 – Hydraulic scheme.

In Fig. 2, p_S and Q_S are supply pressure and flow rate. The arrows in the pipeline indicate the positive flow sense. p_1, p_2, p_3 and p_4 are the pressures on the valve connections. Q_1, Q_2, Q_3 and Q_4 are the flow rates. p_A and p_B are the pressures in chambers A and B, A_e and A_c are the areas of the embolus and the crow, F_a is the force acting on the rod, and $\dot{l}_a$ is the piston speed. For a simpler kinematics analysis of the platform, l_a is the distance between the centers of the actuators mounting joints.

From the measured platform position, the actual actuators position l_a is calculated. The controller compares the actual positions with the desired ones and changes the valve rotor angle θ_V proportionally to the error.

MODELING

In the study of the platform kinematics three references frames are defined, F fixed to the base, R attached to the main crosshead and S attached to the moving platform. The rotation between the frames are summarized by the following indication,

$$\underset{\substack{\text{Fixed}\\\text{Base}\\(x,y,z)}}{F} \xrightarrow{\beta(y)} \underset{\substack{\text{Main}\\\text{Crosshead}\\(x',y,z')}}{R} \xrightarrow{\alpha(x')} \underset{\substack{\text{Moving}\\\text{Platform}\\(x',y'',z'')}}{S}$$

Where β is the angle of rotation around *y-axis* and α is around *x'-axis*. Both angles are measured directly using angular transducers. Due to symmetries of the moving platform and the load, theirs inertia matrix about its center of

mass is given by,

$$ {}^{S}\boldsymbol{I}_{P} = \begin{bmatrix} I_{1P} & 0 & 0 \\ 0 & I_{1P} & 0 \\ 0 & 0 & I_{3P} \end{bmatrix}, \; {}^{S}\boldsymbol{I}_{L} = \begin{bmatrix} I_{1L} & 0 & 0 \\ 0 & I_{1L} & 0 \\ 0 & 0 & I_{3L} \end{bmatrix} \tag{1,2} $$

The vector of angular momentum of the moving platform and the load using S frame about its center of gravity is introduced by,

$$ {}^{S}\boldsymbol{H}_{P} = {}^{S}\boldsymbol{I}_{P} \, {}^{S}_{F}\boldsymbol{\omega}_{S}, \; {}^{S}\boldsymbol{H}_{L} = {}^{S}\boldsymbol{I}_{L} \, {}^{S}_{F}\boldsymbol{\omega}_{S} \tag{3,4} $$

where ${}^{S}_{F}\boldsymbol{\omega}_{S}$ is the angular velocity vector of the platform in body coordinates. The linear momentum vector of the platform and the load is given by Eq.(5) and (6) using S frame,

$$ {}^{S}\boldsymbol{G}_{P} = m_{P} \, {}^{S}\boldsymbol{v}_{P}, \; {}^{S}\boldsymbol{G}_{L} = m_{L} \, {}^{S}\boldsymbol{v}_{L}. \tag{5,6} $$

Equation (7) shows the angular momentum of the system composed by the moving platform and the embarked load, about the center of the main crosshead, which is a fixed point, using S frame (Weber, 2015).

$$ {}^{S}\boldsymbol{H}_{O} = {}^{S}\boldsymbol{H}_{P} + {}^{S}_{O}\tilde{\boldsymbol{r}}_{P} \, {}^{S}\boldsymbol{G}_{P} + {}^{S}\boldsymbol{H}_{L} + {}^{S}_{O}\tilde{\boldsymbol{r}}_{L} \, {}^{S}\boldsymbol{G}_{L} \tag{7} $$

where ${}^{S}_{O}\tilde{\boldsymbol{r}}_{P}$ and ${}^{S}_{O}\tilde{\boldsymbol{r}}_{L}$ are the tilde matrices of the position vector of the platform and load CM using S frame. Using Euler's Law, Eq. (8) gives the torque ${}^{S}\boldsymbol{M}_{O}$ acting on the moving platform.

$$ {}^{S}\boldsymbol{M}_{O} = {}^{S}\dot{\boldsymbol{H}}_{O} + {}^{S}_{F}\tilde{\boldsymbol{\omega}}_{S} \, {}^{S}\boldsymbol{H}_{O} \tag{8} $$

The torque acting on the moving platform is generated by the force vector of the actuators, by the gravity force and by the universal joint constrains, as shown in Eq. (9).

$$ {}^{S}\boldsymbol{M}_{O} = {}^{S}\boldsymbol{T}^{F} \left(\left(m_{P} \, {}^{F}_{O}\tilde{\boldsymbol{r}}_{P} + m_{L} \, {}^{F}_{O}\tilde{\boldsymbol{r}}_{L} \right) {}^{F}\boldsymbol{g} + {}^{F}_{O}\tilde{\boldsymbol{r}}_{C31} \, {}^{F}\boldsymbol{F}_{a1} + {}^{F}_{O}\tilde{\boldsymbol{r}}_{C32} \, {}^{F}\boldsymbol{F}_{a2} \right) + {}^{S}\boldsymbol{M}_{J} \tag{9} $$

where ${}^{S}\boldsymbol{T}^{F}$ is the rotation matrix that leads from F to S frame, m_{P} and m_{L} are the platform and the load masses, ${}^{F}\boldsymbol{g}$ is the gravity vector, ${}^{F}_{O}\tilde{\boldsymbol{r}}_{C31}$ and ${}^{F}_{O}\tilde{\boldsymbol{r}}_{C32}$ are the tilde matrices of the position vector of the points C_{31} and C_{32}, and ${}^{S}\underline{M}_{J}$ is the torque due to the universal joint constraint, given by Eq. (10).

$$ {}^{S}\boldsymbol{M}_{J} = {}^{S}\boldsymbol{T}^{R} \begin{bmatrix} 0 \\ 0 \\ M_{J} \end{bmatrix} \tag{10} $$

where ${}^{S}\boldsymbol{T}^{R}$ is the rotation matrix that leads from R to S frame.

Equation (11) gives the force magnitude of the hydraulic actuator 1 (Jelali and Kroll, 2003).

$$ F_{a1} = p_{A1} A_{e} - p_{B1} A_{c} - F_{f} - m \ddot{l}_{a1} \tag{11} $$

where the index "1" denotes actuator 1, m is the assembly mass which moves with the piston, and F_{f} is the friction force. Changing the index from 1 to 2 on Eq. (11) the force on the second actuator is obtained.

For this kind of numerical simulation, the friction force is well represented as a function of the actuator speed using

a Stribeck curve. The good result is due to the fact that in the analyzed conditions slip velocity on the actuator is significant and a relative small amount of static/kinetic friction appears in the transition (Piatkowski, 2014). A more precise model, like LuGre model, shows the time dependence of the friction and could be used in a more general condition or for real time friction compensation (Yao, 2015).

In the present work, the friction force is obtained experimentally at constant actuator speed, without a load, the fitted function used (continuous blue line) is depicted in Fig. 3 with the experimental data (vertical bars).

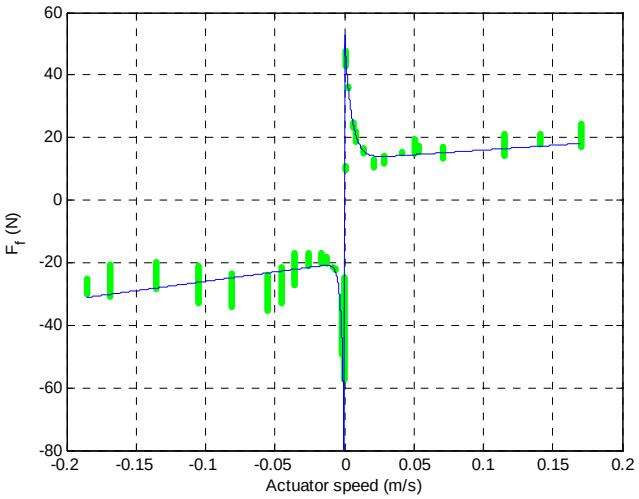

Figure 3 – Actuator friction force.

The vertical bars have this shape because the experiment is performed for a discrete number of actuator speeds and the variation is due to noise and inaccuracy of the used model.

The pressure drop trough a PDHV is calculated using a variable-area orifice model (Manring, 2005),

$$Q_{ij} = \alpha_{Dij} A_{ij} \sqrt{\frac{2}{\rho}\left|p_i - p_j\right|}\, sign\left(p_i - p_j\right). \tag{12}$$

Q_{ij} is the flow rate between connections *i* and *j*, where these indexes vary from *1* to *4* accordingly to the valve connection. α_{Dij} is the discharge coefficient. A_{ij} is the orifice area, which is a function of the valve rotor angle θ_V. In this work, the pipeline pressure loss due to friction is negligible, and it is not considered. But it is considered that the pump is capable of maintaining constant supply pressure during the experiments. This hypothesis was validated.

CONTROLLER

The platform controller is a decentralized proportional controller, hence the position control of each actuator is independent. Figure 4 depicts the control loop.

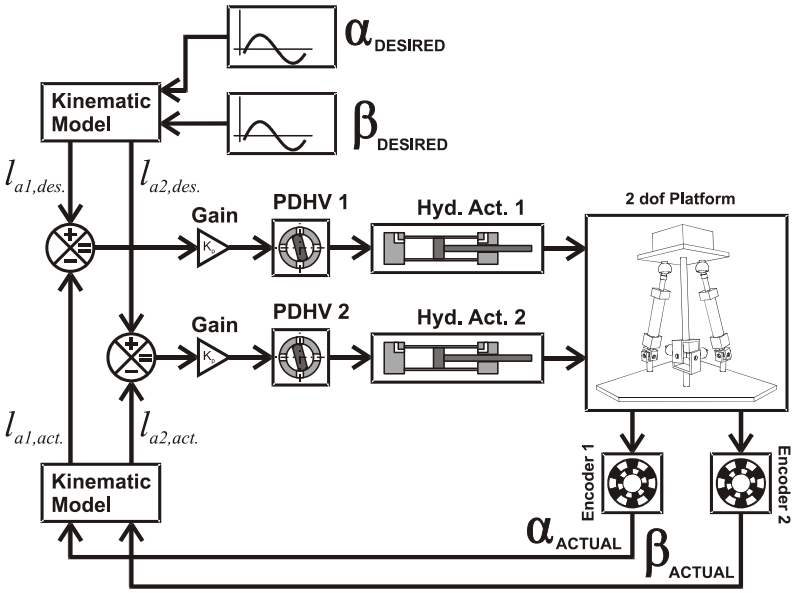

Figure 4 – 2 dof Platform Controller.

The control loop receives a desired angular position for the main universal joint of the platform. Using the kinematic model, the desired actuators positions are calculated and compared with the actual positions. The errors are multiplied by a gain and sent to the PDHV controller. The PDHV controller has an open loop to control a stepper motor attached to the valve rotor. Accordingly to the rotor position, the oil flow to the actuators changes, hence its position changes and the orientation of the platform changes.

The data acquisition system (DAQ) consist in two customized microcontrolled circuits. One, receives the sensors data, sends these data to a computer with a MATLAB running script. The other one receives the desired valves positions from MATLAB script and sends it to the valves controllers. The valve controllers are a variable frequency open loop microcontrolled circuit specially built for the PDHV with *25kHz* control frequency. Figure 5 shows the DAQ operation scheme.

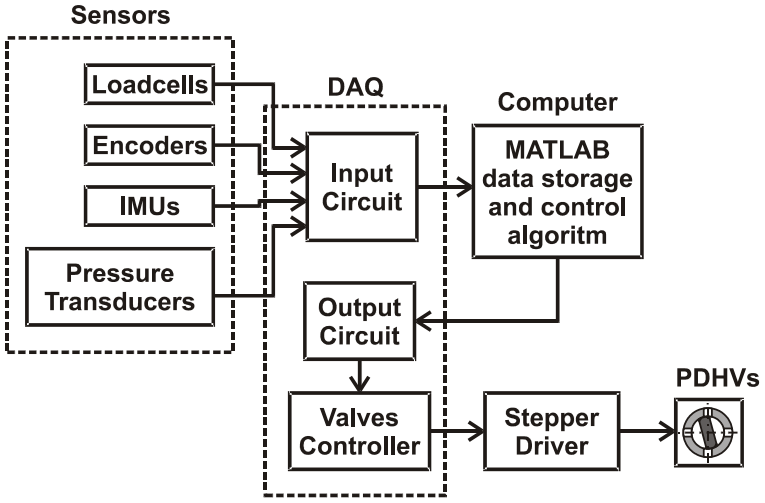

Figure 5 – DAQ system.

The input circuit has an acquisition frequency of *50Hz*, and it is therefore the control frequency. The MATLAB script runs the control algorithm. Hence the time between receiving the sensor data and the response of output variables depends on the complexity of the algorithm and computer speed. For this simple algorithm the delay is less than *1ms*, or about *5%* of the control period.

SIMULATION AND EXPERIMENTS

The experimental data are compared with the numerical simulation and the desired position. The trajectory is defined using the articulation angle θ and the ϕ angle between the *-y-axis* and the projection of *z''-axis* on the *xy-plane*. These angles are shown in Figure 6.

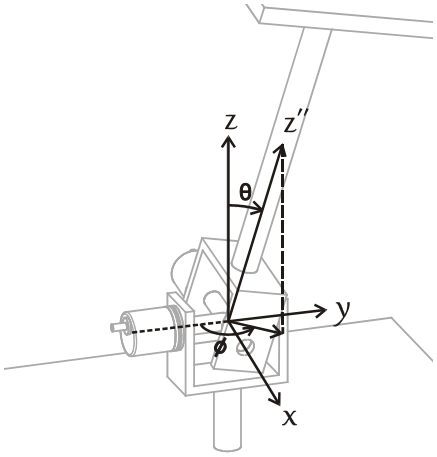

Figure 6. θ and ϕ definition

In the analyzed case, $\theta = 10^o$ and the angle ϕ changes with constant angular velocity $\dot{\phi} = \pi\, rad/s$ from π to 3π.

Table 1 shows same parameters of the platform and the load.

Table 1 – Parameters

Parameter	Value
l_P	$260.0 \cdot 10^{-3} m$
m_P	$4.52 kg$
I_{1P}	$75.7 \cdot 10^{-3} kgm^2$
I_{3P}	$16.9 \cdot 10^{-3} kgm^2$
l_L	$421.1 \cdot 10^{-3} m$
m_L	$17.32 kg$
I_{1L}	$53.6 \cdot 10^{-3} kgm^2$
I_{3L}	$45.8 \cdot 10^{-3} kgm^2$
${}^{F}\underline{g}$	$\begin{bmatrix} 0 & 0 & -9.81 \end{bmatrix}^T m/s^2$
${}^{S}_{O}\underline{r}_{C31}$	$\begin{bmatrix} -65 & 0 & 207.9 \end{bmatrix}^T \cdot 10^{-3} m$
${}^{F}_{O}\underline{r}_{C21}$	$\begin{bmatrix} -135 & 0 & -30 \end{bmatrix}^T \cdot 10^{-3} m$
${}^{S}_{O}\underline{r}_{C32}$	$\begin{bmatrix} 0 & -65 & 207.9 \end{bmatrix}^T \cdot 10^{-3} m$
${}^{F}_{O}\underline{r}_{C22}$	$\begin{bmatrix} 0 & -135 & -30 \end{bmatrix}^T \cdot 10^{-3} m$

Figure 7 shows α and β the experimental(Act) data compared with the numerical simulation(Sim) and the desired position(Des).

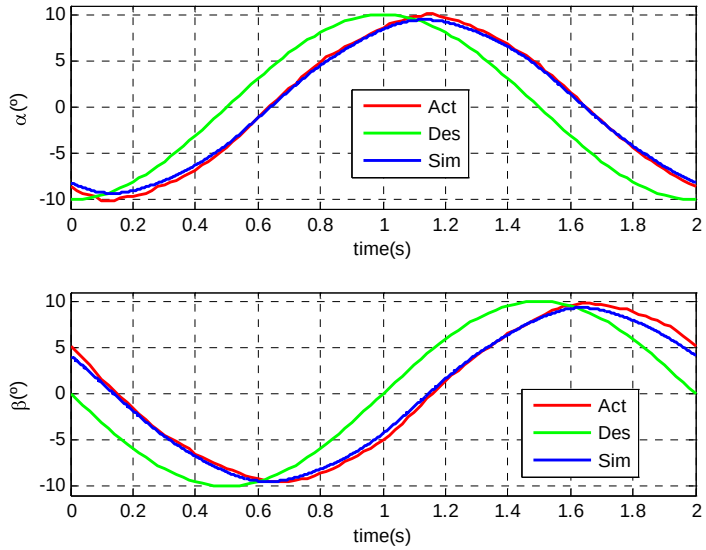

Figure 7 – Simulated and Experimental platform orientation.

The deviation between α simulated and the experimental result is *2,2º* in maximum and *1,2º* in average. The β deviation if *1.8º* in maximum and *0.9º* in average. In this case, Figure 8 shows the actuators length where the plots limits are the actuator limits.

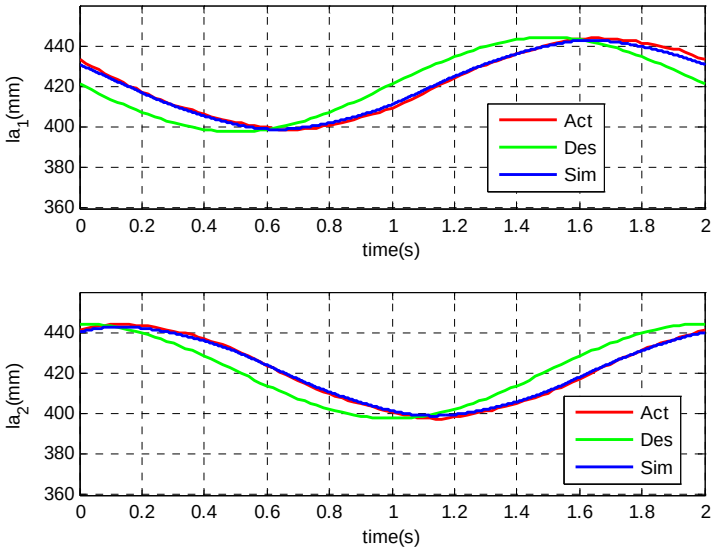

Figure 8 – Simulated and Experimental platform actuator length.

The average error between simulated and the experimental actuators length result is *2mm*, and this error achieves *4mm* for actuator one and *5mm* for actuator two in the maximum. The top view of the table center trace can be seen in Figure 9 with the platform limits(Bound).

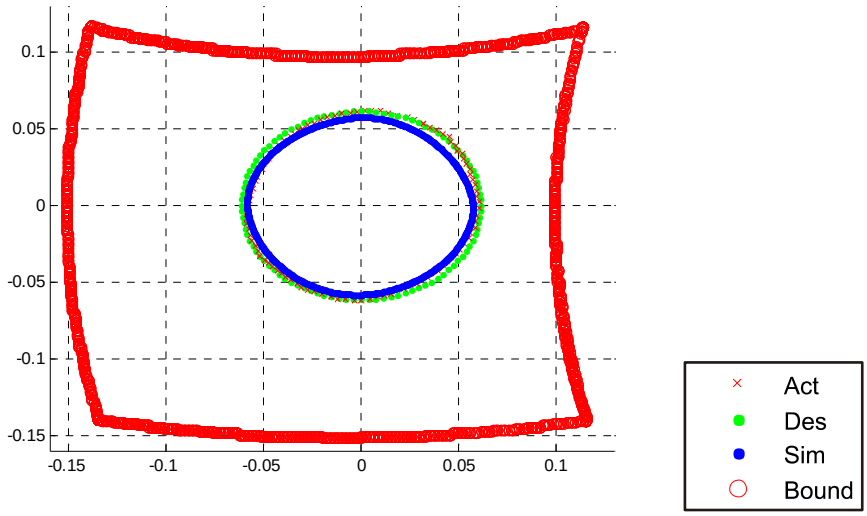

Figure 9 – Top view of the platform table centre trace.

The deviations between simulated and the experimental results are mainly due two model simplifications and platform assembly problems, like backlash and joint friction. The main model simplifications are no friction losses in the pipelines, no actuators inertia and an actuators friction dependent of speed only. The difference between actual, or the simulated, and the desired position is due the extremely simple control algorithm. This proportional control with bigger gain leads to stability problems, mainly chattering.

CONCLUSIONS

In this work, a novel proportional valve was proposed to control a 2dof platform with two linear actuators. For the purpose of simulating the motion of the platform, its kinematics and dynamics model was presented. The modeling of the hydraulic valves and the actuators was also shown. The control diagram has presented a simple decentralized proportional control based on the actuators displacement error. An experimental device validated the numerical results on a path tracking problem. The developed DAQ system was also depicted.

The replacement of the universal joint for a constant velocity joint is in progress. Furthermore, a control algorithm based on the inverse dynamics is being developed to control the platform motion.

REFERENCES

Cardozo, W.S. and Weber, H.I., 2015, Analysis and Development of a Parallel 2 DOF Manipulator, Proceedings of the 23th Brazilian Congress of Mechanical Engineering.

Ghosh, B.B., Sarkar, B.K. and Saha, R., 2014. Realtime performance analysis of different combinations of fuzzy–PID and bias controllers for a two degree of freedom electrohydraulic parallel manipulator, Robotics and Computer-Integrated Manufacturing, 34, 62–69.

Jelali, M. and Kroll, A., 2003. Hydraulic Servo-systems Modelling, Identification and Control, Springer, London, 2nd edition.

Manring, N., 2005. Hydraulic control systems, John Wiley & Sons, New Jersey, USA.

Piatkowski, T., 2014. Dahl and LuGre dynamic friction models — The analysis of selected properties, Mechanism and Machine Theory 73 91–100.

Taghirad, H.D., 2013. Parallel Robots Mechanics and Control, Taylor & Francis Group, Florida.

Watson, I., Prusty, B.G. and Olsen, J., 2013. Conceptual design optimisation of a constant-velocity coupling, Mechanism and Machine Theory, 68 18–34.

Weber, H.I., 2015. “Raciocinando Dinâmica de Rotação”. Book under development, not published yet.

Wekerle, T., Barbosa, E.G., Batagini, C.M., Costa, L.E.V.L. and Trabasso, L.G., 2016, Brazilian Thrust Vector Control System Development: Status and Trends, 52nd AIAA/SAE/ASEE Joint Propulsion Conference, Salt Lake City, UT, USA.

Wekerle, T., Barbosa, E.G., Batagini, C.M., Costa, L.E.V.L. and Trabasso, L.G., 2016. Closed-loop actuator identification for Brazilian Thrust Vector Control development, Proceedings of the 20th IFAC Symposium on Automatic Control in Aerospace, Sherbrooke, Quebec, Canada.

Yao, J., Deng, W. and Jiao, Z., 2015. Adaptive Control of Hydraulic Actuators With LuGre Model-Based Friction Compensation, IEEE Transactions On Industrial Electronics, Vol. 62, No. 10.

RESPONSIBILITY NOTICE

The following note must be added in this last section:

The author(s) is (are) the only responsible for the material included in this paper.